Journal of Applied Sciences and Nanotechnology

Study of the Physico-Chemical Properties of Sol-Gel (Er, Yb) Doped TiO₂ Nanoparticles Prepared with a Novel Protocol

[1,2]I. Benammar*, [3]R. Salhi, [4]J. -L. Deschanvres, [2]R. Maalej

[1]LAMA, National School of Engineers of Sfax, University of Sfax – Tunisia

[2]LaMaCoP, Faculty of Sciences of Sfax, University of Sfax – Tunisia

[3]LEPMI, Grenoble INP, University of Savoie-Mont Blanc – France

[4]LMGP, Grenoble INP, University of Grenoble – France

ARTICLE INFO

Corresponding Author:
I. Benammar
benammar.ikram@yahoo.fr

ABSTRACT

This work describes the systematic preparation of doped and undoped TiO₂ with Er and/or Yb nanoparticles by hydrothermal-assisted sol-gel method with supercritical drying of ethanol, followed by systematic calcination steps at 500°C, 800°C and 1000°C for 2 h. Structural investigation of these powders by XRD shows that our samples are crystalline with a tetragonal structure and an anatase phase well crystallized at 500°C. Annealing at 800°C shows a transformation of the anatase phase into the rutile phase, which is well crystallized at 1000°C. XRD analysis shows that the dopants are incorporated into the TiO₂ network without phase separation in these nanoparticles. The study of the grain sizes has shown that they have a nanometric size of about 8-12 nm and that their size decreases with Er and/or Yb doping. The elemental analyzes with micro-EDX using SEM confirmed the presence of chemical elements in the TiO₂ nanoparticles with the expected atomic ratios. Examination of the SEM images confirmed the XRD observations. They also prove that the nanoparticles are spherical. Optical analysis with excitation at 488 nm shows the presence of three emission bands in the green and red regions. The heat treatment improves the optical, structural and spectroscopic properties and removes impurities due to the preparation conditions.

1. Introduction

In recent years, Titanium dioxide (TiO₂) nanoparticles (NPs) have attracted much attention as a candidate for a vast number of applications [1] due to their excellent optical and electronic properties [2]. It provided high chemical stability [3], excellent biocompatibility [4, 5], nontoxicity and low cost [6]. Studies have reported that TiO₂ nanoparticles with high refractive index and high surface area could potentially be useful in many different applications, such as gas sensors [7-12], photocatalytic activities [13, 14], electronics, and renewable energy generation [15-17]. There are three crystalline forms of TiO₂: anatase (tetragonal), rutile (tetragonal) and brookite

(orthorhombic). Recently, considerable interest has been in synthesising titanium dioxide nanoparticles with pure anatase phase [18]. As reported, the anatase phase is the more favourable structure than the two phases (rutile and brookite). It has high photoactivity [19, 20] due to its wide band gap, high specific surface area and low recombination rates of electron-hole pairs [21, 22]. Zhu *et al.* [23] identified the domains of stability of the three varieties anatase, rutile and brookite produced by sol-gel, depending on the size of the crystallites. The anatase is stable for a size less than 4.9 nm, the brookite for a size between 4.9 and 30 nm and the rutile for a size greater than 30 nm. Zhang *et al.* [24] have shown that the anatase is more stable than the rutile when the grain size is less than 14 nm. In the work by Saranto Polos, the critical size of the anatase-rutile transition is 16 nm, while the necessary phase transition size calculated from thermodynamic data is 14 nm [25, 26]. The two approaches lead to very similar critical transition sizes. Banfield *et al.* [27] have shown that the anatase phase is stable for nanocrystals smaller than 11 nm. Between 11 and 35 nm, the stable phase is the brookite, and the rutile is stabilised for sizes greater than 35 nm. The titanium dioxide in its anatase form has a band gap of 3.23 eV (384 nm), in its rutile form a gap of 3.02 eV (411 nm) and in its brookite form, a gap of 3.4 eV [28]. However, due to its relatively large band gap (3.2 eV), TiO_2 can only be activated by UV light, which limits its practical applications. The utilisation of rare earth (RE) ion-doped nanoparticles has gained significant attention in pursuing novel functionalities, particularly optics. Incorporating rare earth (RE) elements into the semiconductor material offers a range of advantageous outcomes. Firstly, it allows the semiconductor to manifest a reduced absorption threshold for photons with low energy. Secondly, as substantiated by prior investigations, it impedes the rate at which electron-hole pairs recombine by generating transient traps [29]. Moreover, the presence of RE elements reduces semiconductor particles' size and agglomeration tendency, as evidenced by studies [30]. Additionally, utilising rare earth leads to an upconversion phenomenon, wherein the conversion of multiple low-energy photons to high-energy photons occurs within the near-infrared to UV/visible range. This effect has been documented in various investigations [31-33]. Among the rare earth elements, erbium (Er^{3+}) and ytterbium (Yb^{3+}) have garnered considerable attention for their photoluminescence properties when used as dopants in a TiO_2 matrix. Reszczynska *et al.* [34] studied the visible light activity of TiO_2 photocatalysts doped with rare earth metals (Er^{3+}, Yb^{3+}, or Er^{3+}/Yb^{3+}). Their findings indicate that Er-Yb:TiO_2 facilitates phenol degradation in an aqueous solution under visible light irradiation. The choice of Er^{3+} as a promising candidate is supported by its infrared emission at 1535 nm [35]; it shows strong fluorescence at this wavelength [36]. The green and red emission at 550 and 670 nm has been observed with excitation at 975 nm [37]. The Yb^{3+} ions are interesting as a sensitiser of energy transfer from infrared to visible upconversion and infrared lasers [38]. The erbium-ytterbium co-doping promotes up-conversion mechanisms and the energy transfer phenomena between neighbouring ions. Thus, it has the advantage of involving a lower number of phonons and a lower frequency, improving the overall luminescence efficiency [39]. This work uses a hydrothermal-assisted sol-gel process using supercritical ethanol drying to synthesise titania nanoparticles doped with Er and/or Yb. The thermal, structural, morphological, spectroscopic and optical propriety of obtained nanoparticles were studied using TG/DTA, XRD, SEM, TEM, FTIR and micro-Raman.

2. Materials and Methods
2.1 Sample Preparation
2.1.1 Preparation of Pure Solution
The alkoxide precursor utilised in this study is titanium tetra-iso-propoxide (TTIP), denoted by the chemical formula $Ti[OCH(CH_3)_2]_4$, which was procured from the commercial supplier Sigma-Aldrich. TTIP was specifically selected as a metal-organic precursor for synthesising TiO_2 nanoparticles. Preparing the titanium oxide solution involves combining TTIP with a previously prepared methanol and acetic acid solution. The gradual release of water for hydrolysis is achieved through the esterification reaction between acetic acid and methanol. The resulting mixture is then subjected to continuous magnetic stirring at room temperature for 30 minutes, allowing for the dissolution of the TTIP precursor and the uniform blending of the reagents.

2.1.2 Preparation of Doping Solutions

To prepare the solution doped with Er and/or Yb, we followed the same process used to prepare the pure solution. Note that a quantity of erbium (III) nitrate pentahydrate ($Er(NO_3)_3,5H_2O$) and/or a quantity of Ytterbium (III) nitrate pentahydrate ($Yb(NO_3)_3,5H_2O$) (Sigma-Aldrich) has been dissolved. A homogeneous 5% Er and/or 5% Yb and a 5% Er and 10% Yb doped solution were obtained.

2.1.3 Protocol for Drying under the Supercritical Conditions of Ethanol

In the initial step, each sol obtained was subsequently introduced into an autoclave, wherein it was fully immersed in an excessive amount of solvent, specifically ethanol. The autoclave was sealed and subjected to heat and pressure to attain the supercritical state of ethanol, characterised by a temperature of 243°C and a pressure of 63 bar. Subsequently, the supercritical drying process commenced, employing a deliberately gradual temperature increase (referred to as Tc). Once the critical temperature of the solvent was surpassed, a stabilisation period was allowed, followed by a gradual reduction of pressure (referred to as depressurisation) until atmospheric pressure was achieved. Subsequently, a low nitrogen flow was introduced for 5 minutes to eliminate any residual solvent. The system was eventually cooled to room temperature, resulting in the recovery of a titanium dioxide aerogel at the outlet. The obtained nanoparticles in their pure form were subjected to calcination at temperatures of 500°C, 800°C, and 1000°C for 2 hours to examine phase changes. Additionally, the doped nanoparticles underwent treatment at 500°C [39, 40].

2.2 Characterisation Techniques

The thermal properties of the TiO_2 aerogels were investigated using a Setaram SETSYS Evolution 1750 analyser. The thermal cycle gradually heated from room temperature to 800°C, with a heating rate of 10°C per minute. The crystalline structure was analysed through X-ray diffraction (XRD) using a Bruker D8 Advance diffractometer, employing CuKα radiation ($\lambda = 1.54$Å). XRD patterns were obtained within the 2θ range of 20° to 100° with a sampling width of 0.05°. The morphology and particle size of the prepared powders were examined using both Scanning Electron Microscopy (SEM) (FE-SEM, PhilipsXL30) with an accelerating voltage of 20keV and Transmission Electron Microscopy (TEM) (JEOL 2011 microscope) with an accelerating voltage of 200kV. The Fourier Transform Infrared (FT-IR) spectra of doped and undoped TiO_2 nano-powders were acquired at room temperature using a Vertex 70 Bruker spectrometer, covering the frequency range of 200–5000 cm^{-1}. Raman scattering analysis was conducted using a HORIBA/Jobin-Yvon LabRam system and an Olympus confocal microscope detection BX-41 (MicroRaman). Spectra were obtained within the 100-1000 cm^{-1} frequency range, employing a monochromatic laser source with a wavelength of 488 nm (beam diameter between 3 and 5 μm). A reading time of 60 seconds was maintained after initiating the laser. Furthermore, the luminescence of erbium in the visible domain was observed using Raman spectroscopy, with spectra recorded between 500 and 900 cm^{-1}.

3. Results and Discussion

3.1 Thermal Investigation

The properties and the domains of thermal stability of doped and undoped TiO_2 was studied by the TG-DTA analysis, and the results are illustrated in Fig. 1. Thermal gravimetric analyses show two intense mass losses for each thermogram. The first significant weight loss for the TiO_2 sample is located before 138°C of 3.84%. This loss is characterised by the endothermic peak found in the corresponding DTA curves, which could be attributed to the phenomenon of dehydration and deshydroxylation [41]. We note that under the effect of doping and co-doping, the rate of loss slows down and becomes low. The second weight loss characterises an exothermic accident detected in the corresponding DTA curve. It is rapid and significant for TiO_2 located between 138°C and 450°C and 5.7%. It is between 162°C and 450°C of 4.88% for 5%Yb:TiO_2, between 181°C and 455°C of 6.78% for 5%Er:TiO_2, between 170°C and 465°C of 6.2% for 5%Er-5%Yb:TiO_2, between 157°C and 458°C of 6.6% for 5%Er-10%Yb:TiO_2. It could be attributed to partial decomposition and the departure of organic matter [42]. Based on these later curves, two exothermic peaks can be observed for all powders. The first peak, more intense and clearly visible in all the samples, is localised around 288°C for TiO_2. A temperature loss for peaks in other samples was noted. This peak is attributed to the elimination by oxidation of the Ti precursor (alcoxide) and the partial decomposition of organic matter [43]. The second peak is larger, and it begins at approximately 400°C. It can be attributed initially to the remaining organic matter, corresponding to the passage of titanium oxide from the

amorphous phase to the anatase phase [44]. The TiO_2 TG and DTA curve shows thermal stability from 450°C and confirms the good stability of the prepared material.
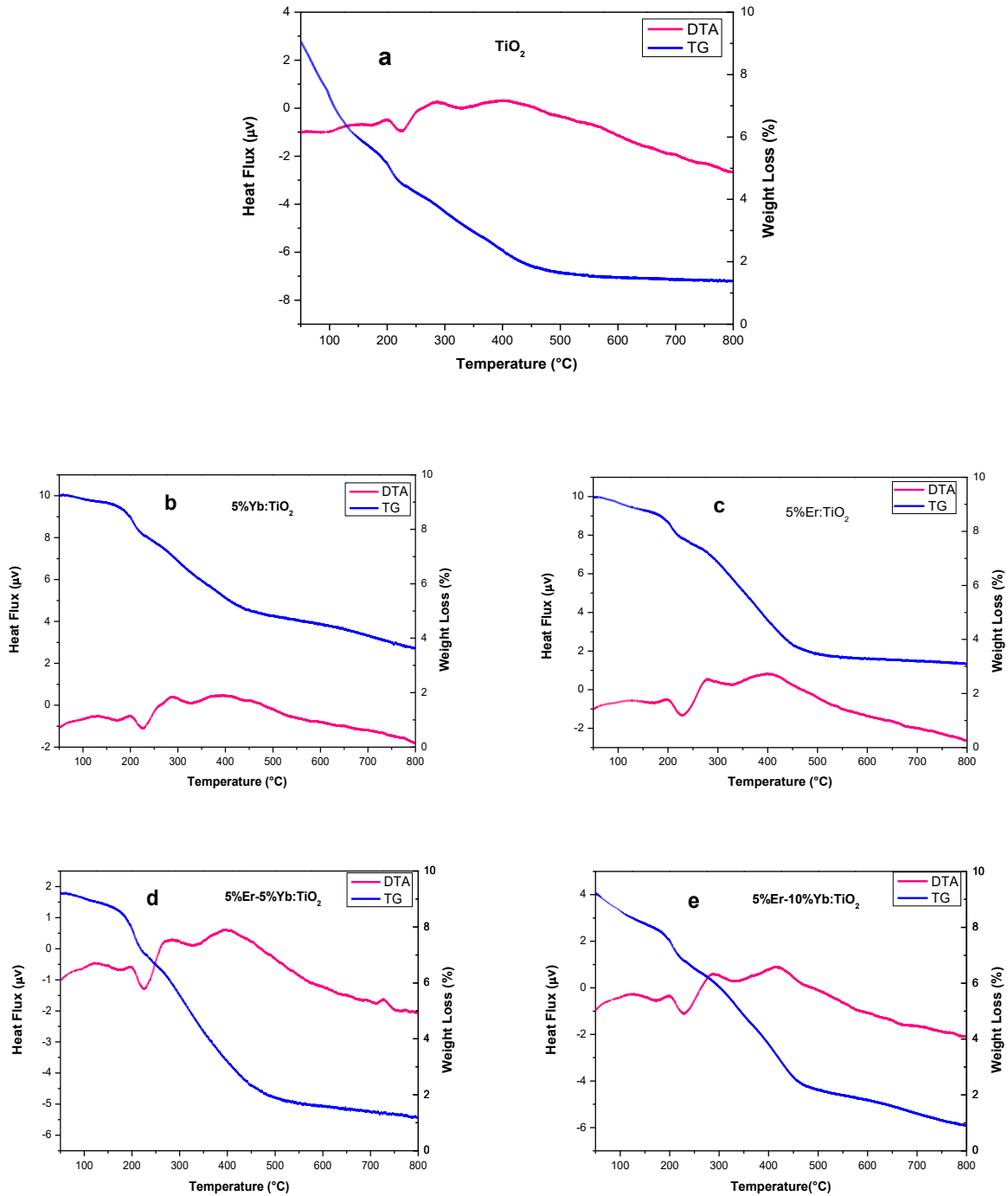

Figure 1: TGA and DTA curve of the (a) TiO_2, (b) 5%Yb:TiO_2, 5%Er:TiO_2, 5%Er-5%Yb:TiO_2 and (e) 5.% Er-10 % Yb:TiO_2 nano-powders.

3.2 Structural and Morphological Investigations

Fig. 2 shows the XRD patterns of the as-prepared pure and doped TiO_2. The diffractogram reveals the presence of several diffraction peaks, meaning the anatase phase of the tetragonal structure of TiO_2, which is compared with Anatase JCPDS 21-1272. These results are in agreement with the work of Park *et al.* [45] and Zhang *et al.* [46]. We note the complete absence of the brookite and the rutile phase. This result is interesting because it proves the efficacy of the experimental protocol developed during the formulation of soil. Indeed, it has been reported that the crystallisation of the gel depends on the working conditions. For example, in the work of M. Ivanda *et al.* [47], a good control of the hydrolysis rate of the precursor Ti (IV)-isopropoxide by an esterification reaction between carboxylic acid (acetic) and alcohol (ethanol) was obtained. It was concluded that the crystallisation of TiO_2 powder obtained by the sol-gel method depends on the acid used; for the acetic acid, the powder is amorphous regardless of the alcohol used, but for the formic acid in addition to the amorphous phase, a number of anatase nanoparticles (the grain size is six nm) has been formed. S. Musé *et al.* [48] obtained a TiO_2 powder crystallised in two phases, anatase and brookite. When the rare earth ions Er and/or Yb are incorporated into the crystal lattice of TiO_2, stress is induced in the system. Indeed, a decrease in intensity at peaks. This indication shows the incorporation of rare earth ions in the TiO_2 matrix without crystal structure distortion. Therefore, we can conclude that doping has no impact on the structure. In Table 1, the crystallite size was obtained by Debye-Scherrer's formula given by equation Eq. (1):

$$D = K\lambda/\beta cos\theta \qquad (1)$$

Where K = 0.9; D represents the crystallite size; λ is the wavelength of Cu (Kα) radiation, and β is the corrected half width of the diffraction peak. The average length of the TiO_2 powders produced in this work is between 7 and 10 nm. This result is fascinating because it proves the interest of the sol-gel synthesis method with drying under supercritical conditions in the development of nanoparticles. It is necessary to remember that this particle size is reported to be essential for optical applications. Indeed, controlling the size of the nanoparticles is essential to minimise the loss of light.
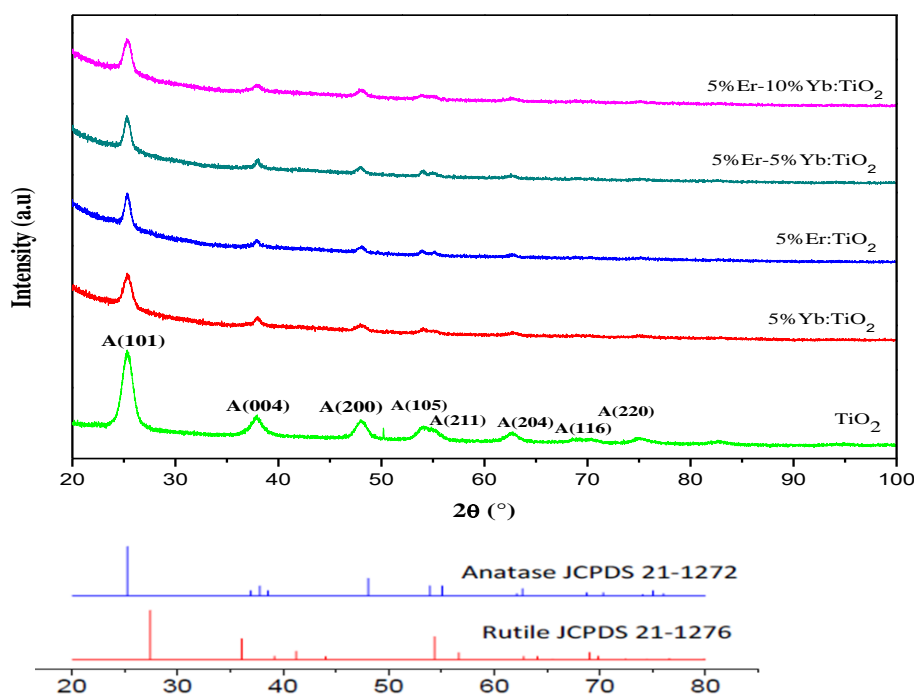

Figure 2: XRD pattern (configuration θ/2θ, KαCu) of doped and undoped TiO_2 nano-powders.

Table 1: Particle size (nm) of doped and undoped TiO_2.

Sample	TiO_2	5%Yb:TiO_2	5%Er:TiO_2	5%Er-5%Yb:TiO_2	5%Er-10%Yb:TiO_2
d (nm)	9.04	6.78	8.76	8.14	8.94

The evolution of the XRD spectra of the prepared nano-powders after the heat treatment at 500°C (Fig. 3) shows an increase in the peak intensity of all the samples and a decrease in the width at mid-height. The peaks become finer than the peaks of samples without annealing. The increase in the peak intensity reflects an increase in the material's crystallinity rate, which is accompanied by an increase in the grain size. The structure obtained is still anatase. The increase in grain size from the Debye-Scherrer formula has been estimated in Table 2.
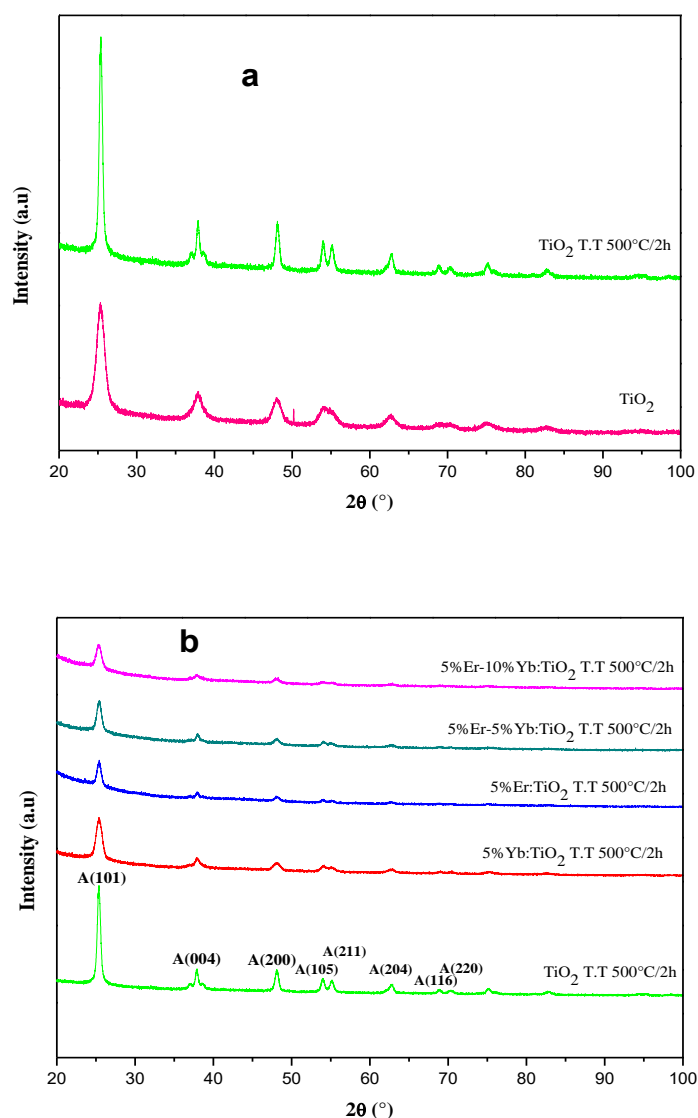

Figure 3: XRD pattern (configuration θ/2θ, KαCu) of (a) TiO_2 and TiO_2 T.T 500°C/2h and (b) doped and undoped nano-powders T.T 500°C/2h.

Table 2: Particle size (nm) of prepared and treated TiO_2 nano-powders with different concentrations of Er/Yb

	TiO₂	5%Yb:TiO₂	5%Er:TiO₂	5%Er-5%Yb:TiO₂	5%Er-10%Yb:TiO₂
untreated	9.04	6.78	8.76	8.14	8.94
T.T 500°C/2h	11.71	9.04	11.65	11.63	11.69

Subsequently, the effect of high temperature treatment on the structural properties of the powders produced by the sol-gel method was studied. Fig. 4 shows the XRD patterns of TiO_2 powders calcined at different temperatures. For the nano-powders annealed at 500°C, the diffraction peaks are attributed to the anatase phase of the tetragonal structure. There is a clear improvement in crystallinity with calcination at 500°C/2h. the Annealing at 800°C reveals a transformation from the anatase phase to the rutile phase with the appearance of the representative peak of the rutile phase ($2\theta=27.30°$). At this temperature, the anatase phase is the majority (75% anatase-25% rutile) with more intense diffraction peaks, which implies an improvement in the crystallinity. According to Chelbi *et al.* [49], the transformation of the anatase-rutile phase occurred at 600°C. In this work, the presence of the rutile phase is confirmed at 800°C. For the powders calcined at 1000°C, only the rutile phase exists and crystallises in the tetragonal system. The average crystallite size of the anatase and the rutile phase was determined using the Debye-Scherrer equation in Table 3. The results shown in Table 3 reveal again that the increase in the annealing temperature is accompanied by an increase in the size of the crystallites that make up each phase of TiO_2.

Table 3: Evolution of the crystallite size of the TiO_2 crystal structure as a function of the calcination temperature.

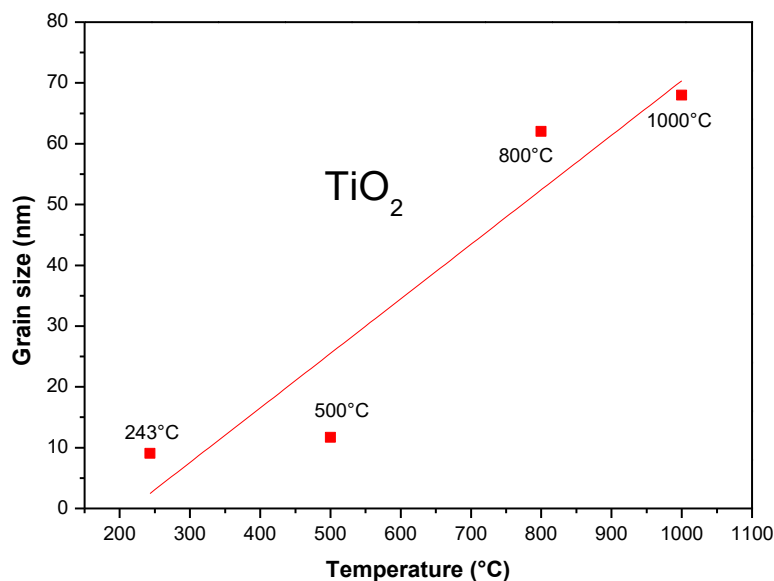| Samples	Crystallite size (nm)		Phase composition (%)	
	Anatase	Rutile	Anatase	Rutile
TiO₂	9.04	-	100	0
TiO₂ T.T 500°C/2h	11.71	-	100	0
TiO₂ T.T 800°C/2h	51	62	74.7	25.3
TiO₂ T.T 1000°C/2h	-	68	0	100

Figure 4: The grain size evolution as a function of the thermal treatment temperature for TiO_2 nano-powders produced by the Sol-Gel process.

Fig. 5 shows the change in grain size as a function of the thermal treatment temperature of the elaborated TiO_2 nanoparticles. This study shows the interest of TiO_2 nano-powders obtained with the sol-gel process from the structural stability and the low grain size magnification that does not exceed the nanoscale.
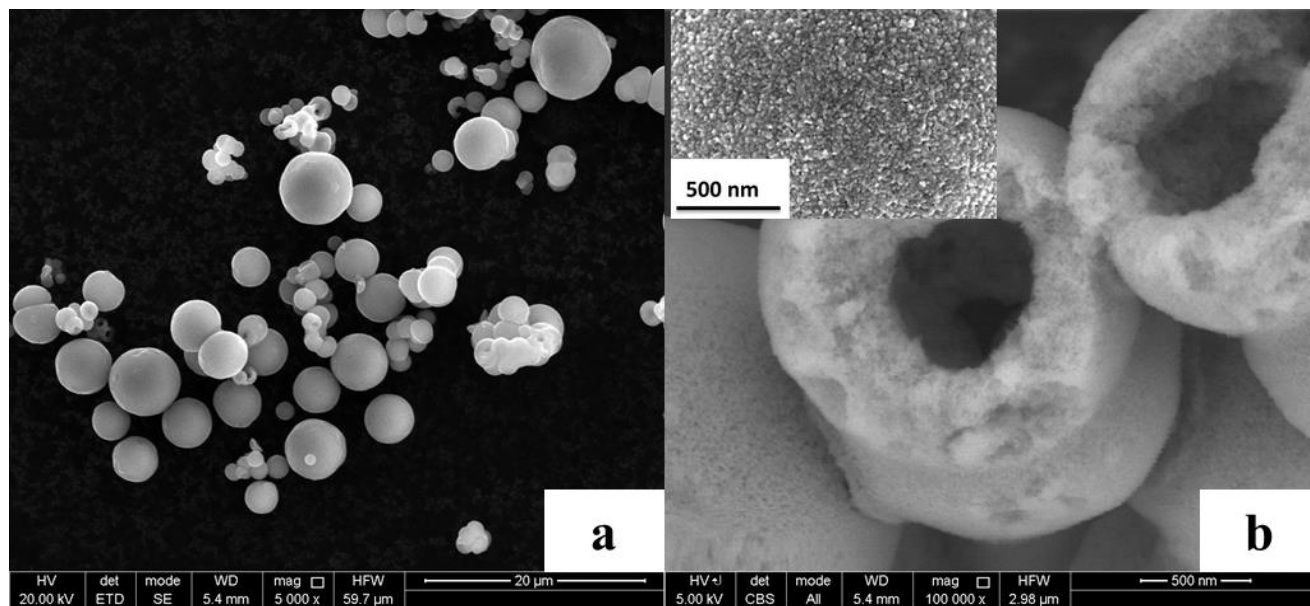

Figure 5: SEM images of TiO_2 powder.

The synthesis of TiO_2 nano-powder, in the absence of annealing, yields spherical particles as depicted in Fig. 6. These spheres are formed through the accumulation of smaller particles measuring approximately 10 nm in diameter. Previous studies have indicated that nanocrystallite spherical aggregates offer advantages over nanoparticles and one-dimensional nanostructures when employed in solar energy conversion systems [50]. The sub-micrometric size of these spherical nanocrystallite aggregates allows for efficient light scattering within the visible light range. Moreover, these aggregates possess a compact internal structure, which enhances the transport capacity of photogenerated electrons compared to a nanoparticle film. As a result, the utilisation of photoelectrodes derived from aggregate structures composed of spherical nanocrystallites demonstrates a conversion efficiency of energy that is comparable to, or even surpasses, those achieved using titania nanoparticles. This can be attributed to the multifunctional nature of these aggregates. Consequently, spherical aggregates represent a highly promising class of materials with the potential to enhance energy conversion efficiency significantly. This potential can be realised by intentionally modifying these aggregates' morphology, size, and porosity [51]. To confirm the existence of Er/Yb elements in the samples subjected to doping, an analysis utilising energy dispersion spectroscopy (EDX) was conducted. A comprehensive breakdown of the compositions of the examined samples can be found in Table 4. The acquired findings unequivocally demonstrate a consistent reduction in the proportion of titanium, accompanied by a proportional escalation in the relative abundance of erbium and/or ytterbium, as the dopant concentration in the solution steadily increases. Fig. 7 shows the TEM image of the TiO_2 nanoparticles co-doped with Er and Yb. It is clear that the nanoparticles prepared with the sol-gel method under the supercritical conditions of ethanol have a spherical shape and in the form of dense aggregates consisting of crystallites. The crystallisers are about 10 to 15 nm in size. The selected area diffraction indicates that the developed TiO_2 nanoparticles are highly crystalline. The spherical shape and nanometric size of the nanoparticles are in agreement with SEM observation and XRD measurements.
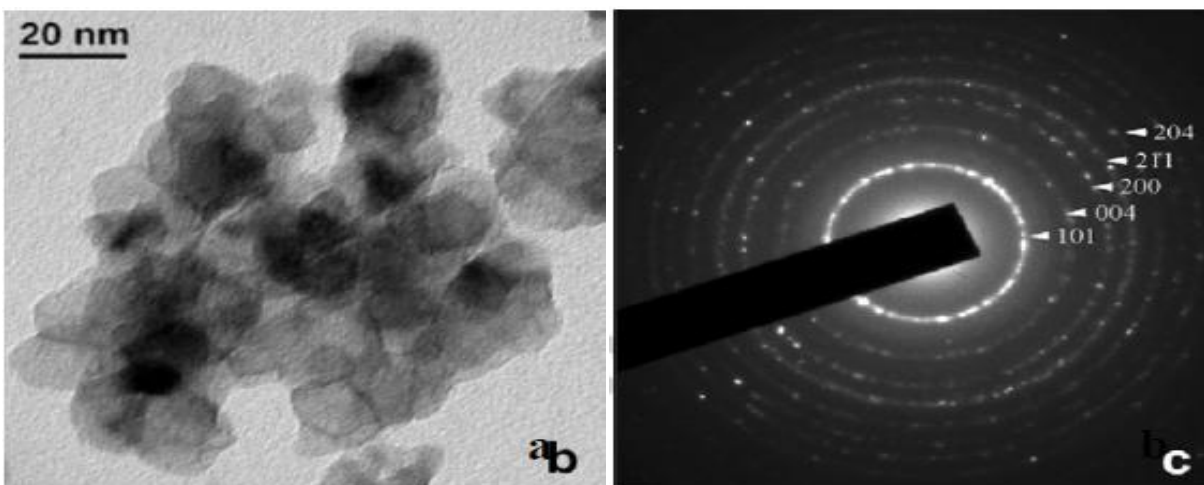
Figure 6: (a) TEM image of 5%Er-5%Yb:TiO_2 T.T 500°C/2h and (b) area electron diffraction images in a selected area (SAED).

Table 4: EDX of doped and undoped TiO_2 nanoparticles.

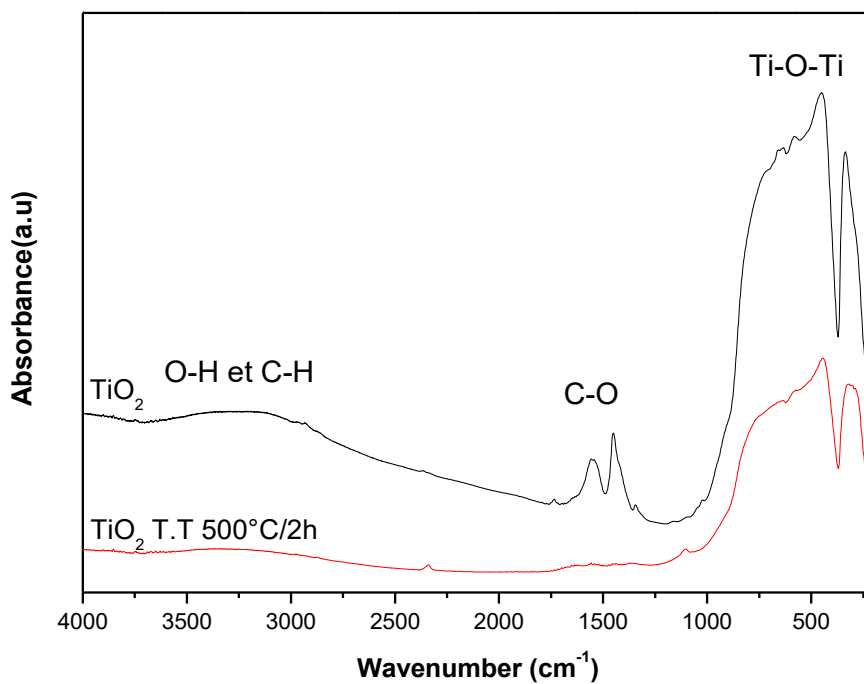| Concentration of Er/Yb in solution (mol.%)	Oxygen (at. %)	Titanium (at. %)	Erbium (at. %)	Ytterbium (at. %)
0 mol.% Er - 0 mol.% Yb	68.37	31.63	00	00
5 mol.% Er - 0 mol.% Yb	69.70	29.06	1.24	00
5 mol.% Er - 5 mol.% Yb	70.05	27.33	1.31	1.31
5 mol.% Er - 10 mol.% Yb	71.32	25.30	1.33	2.05

Figure 7: FTIR spectra of TiO_2 and TiO_2 T.T 500°C nanoparticles.

3.3 Spectroscopic Analysis

Fourier transform infrared spectroscopy (FTIR) was used to identify the individual functional groups in the TiO_2 nanoparticles initially prepared and subsequently annealed (at 500°C) (see Fig. 8). The infrared spectrum showed three distinct absorption bands indicating the presence of specific chemical entities. The appearance of a band between 2300-3700 cm^{-1} is attributed to the vibrations of the OH hydroxyl groups of the water molecule (due to the presence of H_2O that was not completely evaporated) and C-H group [52]. A band between 1300-1800 cm^{-1} can be attributed to the vibrations of organic compounds. The 1600 cm-1 band could be attributed to the C=O bond vibration. These carbonyl groups may be due to hydrocarbon contamination [53]. The absorption peaks between 250 and 700 cm^{-1} with an intense peak corresponding to the vibrations of the Ti-O-Ti bond, which transform into a single band, indicating the disappearance of the alkoxy groups. The spectral band located between 400 and 800 cm^{-1} is attributed to the elongation vibrations υ (Ti-O), which characterises the formation of the Ti-O-Ti bridge. The latter corresponds to the crystallisation of titanium dioxide, which is in agreement with the literature [54]. The calcination of the nanoparticles causes the disappearance of the bands of the carbonyl groups (C-O). During heat treatment at 500°C, the bands due to the vibration of hydroxyl groups (OH) and C-H groups become much weaker, indicating that the elimination of hydroxyl groups and the decomposition of organic solvents is completed, which was in good agreement with the thermal analyses results.
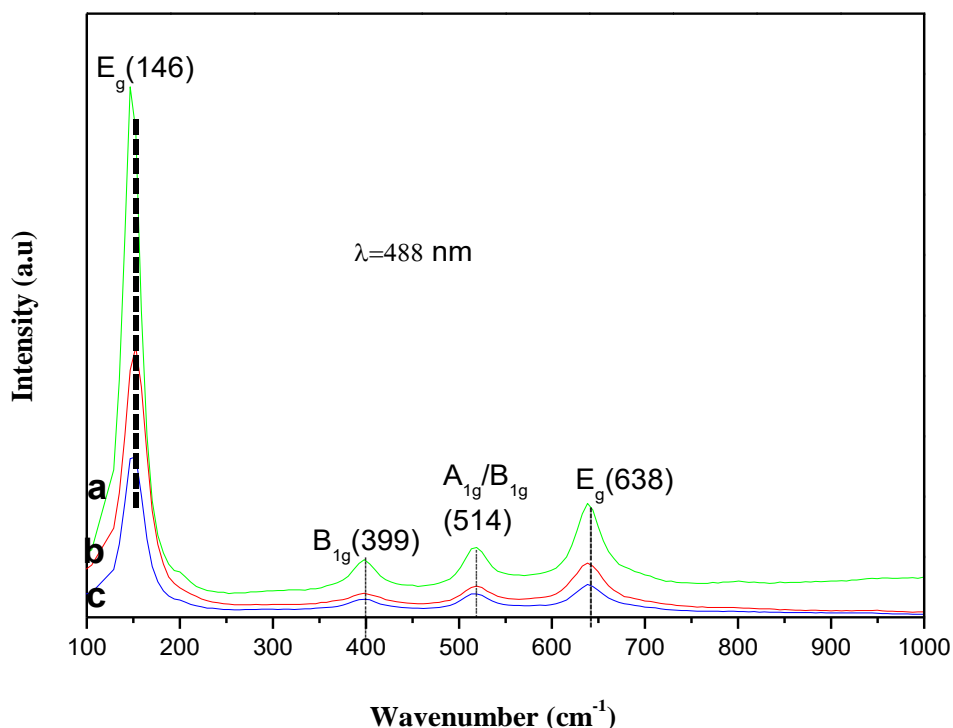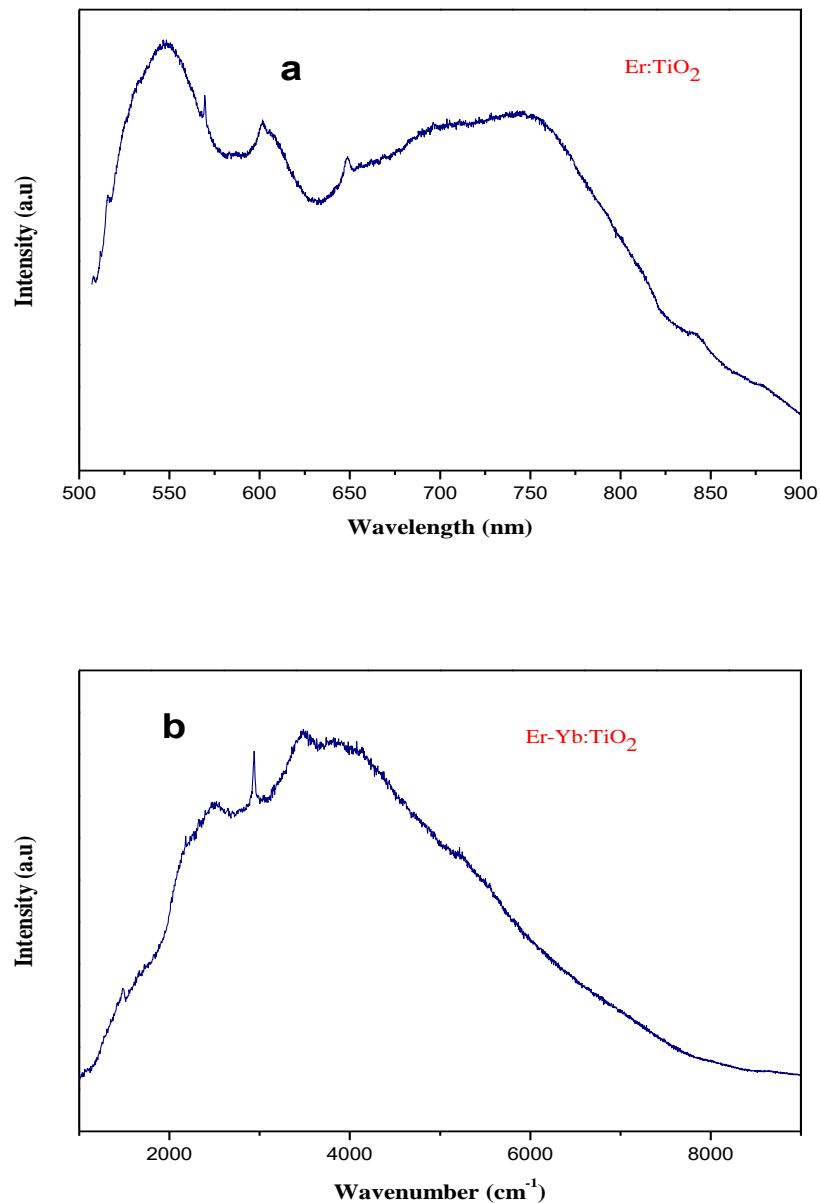

Figure 8: Raman spectra of (a) 5%Er:TiO$_2$, (b) 5%Er-5%Yb:TiO$_2$ and (c) 5%Er-10%Yb:TiO$_2$ nano-powders.

Six vibration modes allowed in Raman spectroscopy (A1g + 2B1g + 3Eg) for anatase TiO$_2$ were reported [55,56].

Fig. 9 of the Raman spectra shows the appearance of peaks corresponding to the vibration modes of an anatase structure (XRD). The anatase phase is characterised by peaks about 146 cm^{-1} (Eg), 399 cm^{-1} (B1g), 514 cm^{-1} (A1g/B1g) and 638 cm^{-1} (Eg). We will be interested in the evolution of the Eg band at 146 cm^{-1} of anatase as a function of the doping concentration because it is the most intense and the finest, which facilitates the observation of its movements. This band is also used in the literature. By comparing the three Raman spectra, it is clear that the Raman bands are moving to the highest wave number. The observed deviation can be attributed to the influence of diminishing nanoparticle dimensions on other properties of the nanoparticles. As the particle size decreases to

the nanoscale, two effects on the vibrational characteristics of these materials may ensue. Firstly, the nanoparticles experience a reduction in volume owing to radial pressure induced by their size, leading to an increase in force constants and, subsequently, a decrease in interatomic distances. In the context of vibrational transitions, the wave number varies in proportion to the square root of the force constant (k1/2), thereby causing the Raman bands to shift towards higher wave numbers due to the augmented force constants. Secondly, the contraction mentioned above induces a decline in the vibrational amplitudes of the neighbouring particles, which can be regarded as a measure of the material's static disorder and thermal vibrations. This decrease in vibrational amplitude, accompanying the reduction in particle size, affects the intensity of the Raman bands. In conclusion, the alterations observed in the Raman spectra of Er- and/or Yb-doped TiO_2 nanoparticles are attributed to the impact of the small nanoparticle size on the force constants and vibrational amplitudes of the neighbouring particle connections [57, 58].
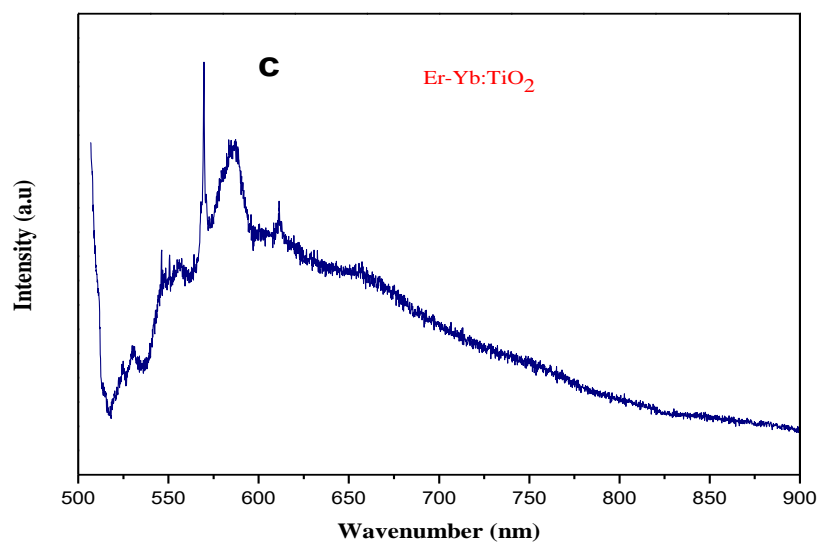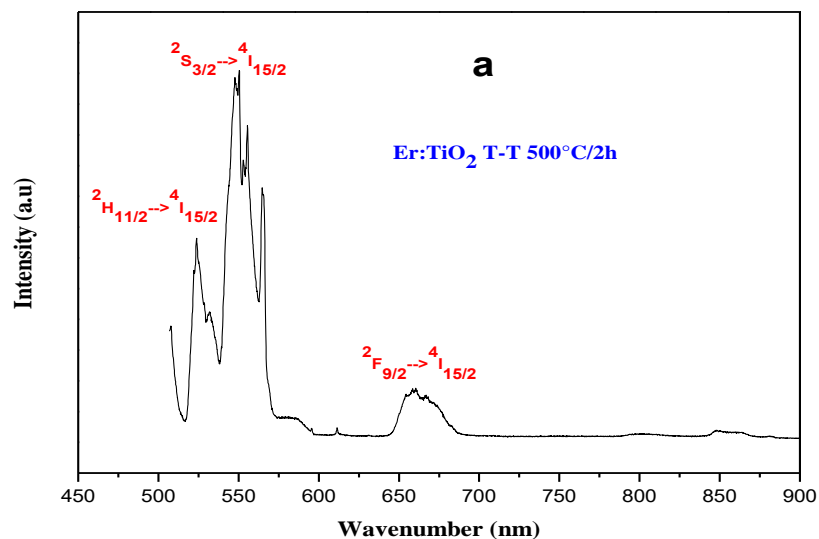
Figure 1: PL spectra of (a) 5%Er:TiO$_2$, (b) 5%Er-5%Yb:TiO$_2$ and (c) 5%Er-10%Yb:TiO$_2$ nano-powders.

3.4 Visible Luminescence of Erbium

The photoluminescence (PL) spectra of untreated nano-powders with excitation under 488 nm at room temperature are shown in Fig. 10. It was observed that the untreated nano-powders exhibit poor luminescence due to organic residues. Wide bands can be seen due to impurities in the elaborated nano-powders. The down-conversion (DC) intensity of 5%Er:TiO$_2$, 5%Er-5%Yb:TiO$_2$ and 5%Er-10%Yb:TiO$_2$ nanoparticles were undetected.
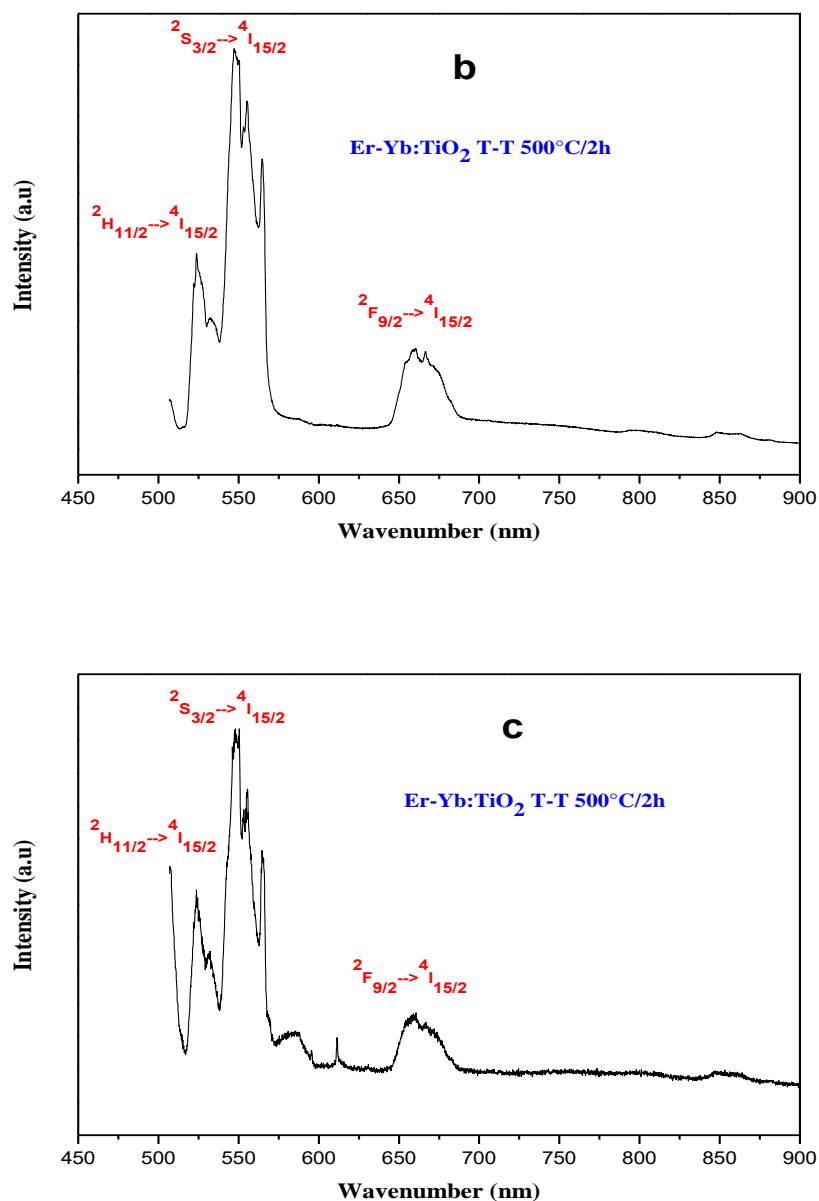
Figure 10: Down conversion emissions of (a) 5%Er:TiO₂, (b) 5%Er-5%Yb:TiO₂ and (c) 5%Er-10%Yb:TiO₂ nano-powders T.T 500°C.

5. Conclusions

Because of the properties required for an active medium giving rise to luminescent materials, the titanium dioxide matrix TiO₂ was chosen for this study thanks to its desired properties: transparency in the visible and near-infrared and the low energy of phonons. The ions used for luminescence are erbium Er^{3+} and ytterbium Yb^{3+} from the rare earth family. The sol-gel method used to develop nano-powders was chosen to manufacture these nanomaterials under supercritical ethanol conditions. The doped and undoped nanoparticles were successfully prepared and annealed at 500, 800, and 1000°C for two hours. These nanoparticles' structural, morphological, spectroscopic, optical, and thermal properties have been studied. The nano-powders obtained crystallise in an anatase structure, and the dopants are incorporated into the TiO₂ matrix without change in structure. These are spherical in shape

and size between 8 and 12 nm. The heat treatment of the elaborated nanoparticles improves their crystallinity and optical properties and eliminates the impurities due to the preparation conditions.

Conflict of Interest
The authors declare that they have no conflict of interest.

References
[1] X. Chen and S. S. Mao, "Titanium dioxide nanomaterials: synthesis, properties, modifications, and applications. Chemical reviews," vol. 107, no. 7, pp. 2891–2959, 2007.

[2] S. Valencia, J. M. Marín and G. Restrepo, "Study of the bandgap of synthesised titanium dioxide nanoparticules using the sol-gel method and a hydrothermal treatment. The Open Materials Science Journal, "vol. 4, pp. 9–14, 2010.

[3] O. Carp, C. L. Huisman and A. Reller, Prog. Solid State Chem., vol. 32, no. 1–2, pp. 33–177, 2004.

[4] W. Han, Y. D. Wang and Y. F. Zheng, "In vivo biocompatibility studies of nano TiO2 materials. In Advanced Materials Research," vol. 79–82, pp. 389–392, 2009.

[5] W. Han, Y. D. Wang and Y. F. Zheng, "In vitro biocompatibility study of nano TiO2 materials. In Advanced Materials Research", vol. 47–50, pp. 1438–1441, 2008.

[6] S. Velázquez-Martínez, S. Silva-Martınez, C.A. Pineda-Arellano, A. Jimenez-Gonzalez, I. Salgado-Transito,' A.A. Morales-Perez and M.I. Pena-Cruz, "Modified sol-gel/hydrothermal method for the synthesis of microsized TiO2 and iron-doped TiO_2, its characterisation and solar photocatalytic activity for an azo dye degradation. Journal of Photochemistry and Photobiology A: Chemistry," vol. 359, pp. 93–101, 2018.

[7] C. H. Han, D. W. Hong, S. Do Han, J. Gwak and K. C. Singh, "Catalytic combustion type hydrogen gas sensor using TiO2 and UV-LED. Sensors and Actuators B: Chemical," vol. 125, no. 1, pp. 224–228, 2007.

[8] J. A. Park, J. Moon, S. J. Lee, S. H. Kim, T. Zyung and H. Y. Chu, "Structure and CO gas sensing properties of electrospun TiO_2 nanofibers. Materials Letters," vol. 64, no. 3, pp. 255–257, 2010.

[9] V. Galstyan, "Porous TiO2-based gas sensors for cyber chemical systems to provide security and medical diagnosis. Sensors," vol. 17, pp. 2947, 2017.

[10] K. P. Priyanka, S. C. Vattappalam, S. Sankararaman, K. M. Balakrishna and T. Varghese, "High-performance ethanol gas sensor using TiO 2 nanostructures. The European Physical Journal Plus," vol. 132, pp. 306, 2017.

[11] J. Tian, G. Yang, D. Jiang, F. Su and Z. Zhang, "A hybrid material consisting of bulk-reduced TiO 2, graphene oxide and polyaniline for resistance based sensing of gaseous ammonia at room temperature. Microchimica Acta, " vol. 183, no. 11, pp. 2871–2878, 2016.

[12] X. Zhang, Y. Gui and X. Dong, "Preparation and application of TiO 2 nanotube array gas sensor for SF 6-insulated equipment detection: A review. Nanoscale Research Letters," vol. 11, pp. 302, 2016.

[13] L. Chen, J. Tian, H. Qiu, Y. Yin, X. Wang, J. Dai, P. Wu, A. Wang, L. Chu, Ceram. Int., vol. 35, no. 8, pp. 3275–3280, 2009.

[14] T. Yazawa, F. Machida, N. Kubo and T. Jin, "Photocatalytic activity of transparent porous glass supported TiO_2. Ceramics International, ", vol. 35, no. 8, pp. 3321–3325, 2009.

[15] H. Yang, K. Zhang, R. Shi, X. Li, X. Dong and Y. Yu, J. Alloys Compd., vol. 413, no. 1–2, pp. 302–306, 2006.

[16] S. Lee, I. S. Cho, J. H. Lee, D. H. Kim, D. W. Kim, J. Y. Kim, H. Shin, J. K. Lee, H. S. Jung, N. G. Park, K. Kim, M. J. Ko and K. S. Hong, Chem. Mater., vol. 22, no. 6, pp. 1958–1965, 2010.

[17] M. A. Behnajady, H. Eskandarloo, N. Modirshahla and M. Shokri, "Investigation of the effect of sol–gel synthesis variables on structural and photocatalytic properties of TiO2 nanoparticles. Desalination," vol. 278, no. 1–3, pp. 10–17, 2011.

[18] M. V. Dozzi and E. Selli, "pecific facets-dominated anatase TiO_2: fluorine-mediated synthesis and photoactivity. Catalysts," vol. 3, no. 2, pp. 455–485, 2013.

[19] J. Liu, Optoelectron. Adv. Mater. Rapid Commun., vol. 5, no. 3, pp. 291–295, 2011.

[20] D. A. H. Hanaor and C. C. Sorrell, "Review of the anatase to rutile phase transformation. Journal of Materials science," vol. 46, no. 4, pp. 855–874, 2011.

[21] S. Mahshid, M. Askari, M. Sasani Ghamsari, N. Afshar and S. Lahuti, "Mixed-phase TiO$_2$ nanoparticles preparation using sol–gel method. Journal of Alloys and Compounds, " vol. 478, no. 1–2, pp. 586–589, 2009.

[22] A. Fujishima, X. Zhang and D. A. Tryk, "TiO2 photocatalysis and related surface phenomena. Surface science reports," vol. 63, no. 12, pp. 515–582, 2008.

[23] Y. Zhu, L. I. Zhang, C. Gao and L. Cao, Journal of Materials Science, vol. 5, pp. 4049–4054, 2000.

[24] Y. Guo, X. Zhang and G. Han, Materials Science and Engineering, vol. 135, pp. 83–87, 2006.

[25] Y. Ug, E. Jung, H. Tae and S. Hong, Materials Letters, vol. 57, pp. 4660–4666, 2003.

[26] B. Jeong, D. P. Norton and J. D. Budai, Solid-State Electronics, vol. 47, pp. 2275–2278, 2003.

[27] E. Jung Kim and S. H. Hahn, "Microstructural changes of microemulsion-mediated TiO2 particles during calcination. Materials Letters," vol. 49, pp. 244–249, 2001.

[28] G. Beaucage, "Small-angle scattering from polymeric mass fractals of arbitrary mass-fractal dimension. Journal of applied crystallography," vol. 29, pp. 134–146, 1996.

[29] M. Fhoula, T. Kallel, M. Messaoud, M. Dammak and E. Cavalli, "Morphological, spectroscopic and photocatalytic properties of Eu^{3+}: TiO$_2$ synthesised by solid-state and hydrothermal-assisted sol-gel processes. Ceramics International, " vol. 45, no. 3, pp. 3675–3679, 2019.

[30] K. Singh, S. Harish, A. Periyanayaga Kristy, V. Shivani, J. Archana, M. Navaneethan, M. Shimomura and Y. Hayakawa, "Erbium doped TiO$_2$ interconnected mesoporous spheres as an efficient visible light catalyst for photocatalytic applications. Applied Surface Science," vol. 449, pp. 755–763, 2018.

[31] A. Maheshwari, S. B. Rai, O. Parkash and D. Kumar, "Effect of crystallisation temperature on luminescence behaviour of Er–Yb: SrO· TiO$_2$ borosilicate glass. Journal of luminescence, " vol. 137, pp. 1–5, 2013.

[32] Y. Yang, C. Zhang, Y. Xu, H. Wang, X. Li and C. Wang, " Electrospun Er: TiO$_2$ nanofibrous films as efficient photocatalysts under solar simulated light. Materials Letters," vol. 64, no. 2, pp. 147–150, 2010.

[33] V. C. Bhethanabotla, D. R. Russell and J. N. Kuhn, "Assessment of mechanisms for enhanced performance of Yb/Er/titania photocatalysts for organic degradation: Role of rare earth elements in the titania phase. Applied Catalysis B: Environmental, " vol. 202, pp. 156–164, 2017.

[34] J. Reszczyńska, T. Grzyb, J. W. Sobczak, W. Lisowski, M. Gazda, B. Ohtani and A. Zaleska, "Visible light activity of rare earth metal doped (Er^{3+}, Yb^{3+} or Er^{3+}/Yb^{3+}) titania photocatalysts. Applied Catalysis B: Environmental," vol. 163, pp. 40–49, 2015.

[35] N. V Gaponenko, O. V Sergeev, E. A. Stepanova, V. M. Parkun, A. V. Mudryi, H. Gnaser, J. Misiewicz, R. Heiderhoff, L. J. Balk and G. E. Thompson, Journal of The Electrochemical Society, vol. 148, pp. 13–16, 2001.

[36] A. J. Kenyon, P. F. Trwoga, M. Federighi and C. W. Pittvol, 1. Phys.: Condens. Matter, vol. 6, pp. 1319-1324, 1994.

[37] A. Patra, C. S. Friend, R. Kapoor and P. N. Prasad, "Fluorescence upconversion properties of Er3+-doped TiO$_2$ and BaTiO$_3$ nanocrystallites. Chemistry of Materials, " vol. 15, no. 11, pp. 3650–3655, 2003.

[38] G. Wang, J. Zhang, S. Xu, S. Dai, L. Hu and Z. Jiang, "Thermal analysis, spectra and laser properties of a new Yb3+-doped multicomponential tellurite-based glass. Journal of luminescence, " vol. 109, pp. 1–7, 2004.

[39] R. Salhi and J. L. Deschanvres, "Efficient green and red up-conversion emissions in Er/Yb co-doped TiO$_2$ nano-powders prepared by hydrothermal-assisted sol–gel process. Journal of Luminescence," vol. 176, pp. 250–259, 2016.

[40] I. Benammar, R. Salhi, J. L. Deschanvres and R. Maalej, "The effect of solvents and rare-earth element (Er, Yb) doping on suspension stability of sol–gel titania nanoparticles. IEEE Transactions on NanoBioscience," vol. 16, no. 8, pp. 718–726, 2017.

[41] H. Yin, Y. Wada, T. Kitamura, T. Sumida, Y. Hasegawa and S. Yanagida, " Novel synthesis of phase-pure nano-particulate anatase and rutile TiO_2 using $TiCl_4$ aqueous solutions. Journal of Materials Chemistry, " vol. 12, no. 2, pp. 378–383, 2002.

[42] M. Kobayashi, V. V. Petrykin, M. Kakihana, K. Tomita and M. Yoshimura, Chem. Mater., vol. 19, no. 22, pp. 5373–5376, 2007.

[43] W. F. Sullivan and S. S. Cole, "Thermal chemistry of colloidal titanium dioxide. Journal of the American Ceramic Society, " vol. 42, no. 3, pp. 127–133, 1959.

[44] D. Bersani, P. P. Lottici, M. Braghini and A. Montenero, Phys. Status Solidi, vol. 170, no. 1, pp. K5–K10, 1992.

[45] S. E. Park, H. Joo and J. W. Kang, "Effect of impurities in TiO_2 thin films on trichloroethylene conversion. Solar energy materials and solar cells, " vol. 83, no. 1, pp. 39– 53, 2004.

[46] X. Zhang and Q. Liu, " Preparation and characterisation of titania photocatalyst co-doped with boron, nickel, and cerium. Materials Letters," vol. 62, no. 17–18, pp. 2589–2592, 2008.

[47] M. Ivanda, S. Music, S. Popovic and M. Gotic, "RD, Raman and FT-IR spectroscopic observations of nanosized TiO_2 synthesised by the sol–gel method based on an esterification reaction. Journal of Molecular structure," vol. 481, pp. 645–649, 1999.

[48] S. Music, M. Gotic, M. Ivanda, S. Popovic, A. Turkovic, R. Trojko, A. Sekulic and K. Furic, Materials Science and Engineering, vol. 47, pp. 33–40, 1997.

[49] S. Chelbi, L. Hammiche, D. Djouadi and A. Chelouche, Association Algérienne de Physique, vol. 2, pp. 69-73, 2015.

[50] R. Salhi, H. Roussel, P. Chaudouet, R. Maalej, M. Fourati and J.-L. Deschanvres, "Growth rate induced high efficient light trapping/photon conversion ZnO: Nd^{3+} nanodisk shaped thin films deposited by AACVD process. Journal of Alloys and Compounds, " vol. 17, pp. 93-97, 2011.

[51] R. Salhi, C. Jimenez, JL. Deschanvres, Y. Guyot, O. Chaix-Pluchery, L. Rapenne, R. Maalej and M. Fourati, "Preparation and microstructural properties of erbium doped alumina–yttria oxide thin films deposited by aerosol MOCVD. Journal of luminescence, " vol. 142, pp. 52–56, 2013.

[52] P. D. Cozzoli, A. Kornowski and H. Weller, "Low-temperature synthesis of soluble and processable organic-capped anatase TiO_2 nanorods. Journal of the American chemical society, " vol. 125, pp. 14539– 14548, 2003.

[53] E. T. Fitzgibbons, K. J. Sladek and W. H. Hartwig, J. Electrochem. Sac: Solid-State Science and Technology, vol. 119, no. 6, pp. 735-739, 1971.

[54] L. S. Hsu, R. Rujkorakarn, J. R. Sites and C. Y. She, J. Appl. Phys., vol. 59, no. 10, pp. 3475-3480, 1986.

[55] B. J. Choi, D. S. Jeong, S. K. Kim, C. Rohde, S. Choi, J. H. Oh, H. J. Kim, C. S. Hwang, K. Szot, R. Waser, B. Reichenberg and S. Tiedke, "Resistive switching mechanism of TiO 2 thin films grown by atomic-layer deposition. Journal of applied physics, " vol. 98, no. 3, pp. 033715, 2005.

[56] T. Ohsaka, F. Izumi and Y. Fujiki, Journal of Raman Spectroscopy, vol. 7, no. 6, pp. 321–324, 1978.

[57] J. Rockenberger, L. Troger, A. Kornowski, T. Vossmeyer, A. Eychmuller, J. Feldhaus and H. Weller, "EXAFS studies on the size dependence of structural and dynamic properties of CdS nanoparticles. The Journal of Physical Chemistry B, " vol. 101, pp. 2691-2701, 1997.

[58] M.A. Marcus, M.P. Andrews, J. Zegenhagen, A.S. Bommannavar and P. Montano, "Structure and vibrations of chemically produced Au 55 clusters. Physical Review B, " vol. 42, pp. 3312-3316, 1990.

[59] J. Sun, Y. Lan, Z. Xia and H. Du, "Sol–gel synthesis and green upconversion luminescence in BaGd2 (MoO4) 4: Yb3+, Er3+ phosphors. Optical Materials," vol. 33, pp. 576-581,2011.

[60] C.S. Lim, "Preparation of CaLa2 (MoO4) 4: Er3+/Yb3+ phosphors via the microwave-modified sol–gel route and the upconversion of their photoluminescence properties. Materials Research Bulletin, " vol. 60, pp. 537-542, 2014.

[61] R. Elleuch, R. Salhi, N. Maalej, J. L. Deschanvres and R. Maalej, Mater. Sci. Eng. B, vol. 178, no. 17, pp. 1124–1129, 2013.

[62] E. Alves, E. Rita, U. Wahl, J. G. Correia, T. Monteiro, J. Soares and C. Boemare, Nuclear Instrum., vol. 206, pp. 1047–1051, 2003.

[63] R. Elleuch, R. Salhi, S. I. Al-Quraishi, J. L. Deschanvres and R. Maalej, "Efficient antireflective downconversion Er3+ doped ZnO/Si thin film. Physics Letters A," vol. 378, pp. 1733–1738, 2014.

[64] B. Dong, D. P. Liu, X. J. Wang, T. Yang, S. M. Miao and C. R. Li, Appl. Phys. Lett., vol. 90, pp. 3–6, 2007.

[65] N. R. Aghamalyan, R. K. Hovsepyan, E. A. Kafadaryan, R. B. Kostanyan, S. I. Petrosyan, G. H. Shirinyan, M. N. Nersisyan, A. Kh. Abduev and A. Sh. Asvarov, Journal of Contemporary Physics, vol. 43, no. 3, pp. 144-149, 2008.